Part Four

Ocean and Atmosphere

17
Air–Sea
Interaction

H. Charnock

17.1 Introduction

In preparing a chapter for a book such as this some nostalgia is excusable, even inevitable. For those who came to the subject, or came back to the subject, after the war there was a bewildering range of work going on. Barber and Ursell were publishing their results on the long-distance propagation of ocean swell, having used an analogue device to estimate the wave spectrum. Sverdrup and Munk had done wartime work on waves too, but by 1947 Munk was writing on a possible critical velocity for air–sea transfer processes and Sverdrup was working up his classical paper on currents driven by the curl of the wind stress. Jacobs was continuing his long-term study of the climatology of energy exchange between sea and air: Budyko was just starting his. Sheppard was publishing his direct determination of the shearing stress by use of a drag plate and Roll was making new wind-profile measurements over the Wattenmeer. Obukhov had already developed the dimensional arguments leading to the Monin–Obukhov length and had contributed to the Kolmogoroff small-scale similarity hypothesis with Onsager and Weizsäcker: in Cambridge, Batchelor was exploring its consequences. Priestley was off to Australia to set up a powerful group on near-surface turbulence, and was making pioneering calculations of the poleward heat and momentum transfer by covariance of wind and temperature fluctuations. Eady was in London working up his idea about baroclinic instability, Charney his at Princeton. Henry Stommel, relatively recently at Woods Hole, was interested in convection in the atmosphere and ocean (it was the time of the Woodcock–Wyman expedition) and had discovered the phenomenon of entrainment into cumulus clouds.

The importance of air–sea interaction to the larger-scale flows of the atmosphere and ocean was in no doubt, though it was a somewhat minority interest. Most of the work at that time concerned the estimation of the surface fluxes of heat, water vapor, and momentum from the only data base then foreseen, namely, the routine observations of temperature (dry bulb, wet bulb, sea) and wind made from the merchant vessels that reported to national meteorological agencies. Given suitable formulas it was thought that one could perhaps calculate the poleward heat transfer by the ocean and make some progress on relating winds to near-surface currents.

There were obvious difficulties of observation over the sea rather than the land but these were compensated for by the importance of the results and by the relative uniformity of the surface, both in space and, due to the high thermal capacity of the ocean, in time. Also the problem was close enough to a laboratory shear flow to allow comparisons with flow in pipes and

channels. Much of the early work therefore concerned itself with the fluid mechanics of the air flow over the sea to a height of, say, 50 m. Since then the concept of air-sea interaction has been much broadened to include consideration of phenomena on larger space and time scales. General problems such as the teleconnections between sea surface temperature anomalies and subsequent weather patterns and specific aspects such as El Niño have been included. One thinks of climate as a complex of interactions between the air, the sea, and the surface of the earth, and in this sense air-sea interaction can be argued to include much of the physics and dynamics of the atmosphere and the ocean. But this review will consider only the small-scale processes by which heat, water, and momentum are transferred near the sea surface. In a fundamental sense the air and the sea interact only in a thin interfacial layer, but it is convenient to consider processes confined to the coupled boundary layers of the atmosphere and the ocean, which, as will be seen, extend typically to a height of 1000 m and a depth of 30 m from the sea surface.

The first section deals with the surface layer of the atmosphere, which constitutes about the lowest tenth of the whole atmospheric boundary layer. This is the only region for which a satisfactory (though empirical) treatment is available in the form of "similarity theory" that relates small-scale properties of the airflow (gradients, turbulence spectra) to the vertical fluxes of momentum, heat, and water vapor.

To get the mean profiles, or the exchange coefficients (which are important in practice), requires boundary conditions within the interfacial layer. These are not at all well understood—observational results are briefly summarized in section 17.3.

Many of the difficulties associated with the interfacial layer are due to the complications introduced by surface waves. The relation between the wind stress (or the aerodynamic roughness) and the surface wave field (or the geometrical roughness) has proved an intransigent problem. Recent advances in our knowledge of the wave spectrum, and of the pressure distribution at the moving sea surface, are indicated in section 17.4.

The development of computer models of the atmosphere, and increasingly of the atmosphere and ocean combined, have much reduced the emphasis on the near-surface meteorological variables. The surface fluxes are no longer related to ships' observations so much as to winds, temperatures, and humidities in the atmosphere and ocean at levels where the flow can be taken to be frictionless and adiabatic. This requires increased understanding of the structure of the boundary layer as a whole. Section 17.5 describes our regrettably limited knowledge of the climatology of the atmospheric boundary layer and of the complicated processes that affect the distribution of density and

wind within it. Some of the processes are similar to those that determine the structure of the oceanic boundary layer: for others, such as clouds, there is no obvious analogy.

17.2 The Surface Layer

The lowest 50 m of the boundary layer of the atmosphere has a special importance and simplicity that together with its accessibility have attracted intensive study. The importance of the surface layer comes from the fact that although its depth is only a small fraction of the whole boundary layer, it is within it that most of the change of wind speed, temperature, and humidity between the free atmosphere and the surface takes place. Its simplicity comes about because the fluxes of momentum, heat, and water vapor undergo only small fractional changes within the surface layer, so they may commonly be regarded as independent of height. For this reason it is convenient to take the fluxes of momentum and potential density as the basic independent variables governing the motion, and to consider the mean gradients and all the properties of the turbulence as being determined by them.

17.2.1 Near-Surface Profiles in Neutral Conditions
Many measurements of the vertical profile of velocity have been made over sites uniform for an upwind distance great compared to the height of observation z in conditions steady for times greater than z/u_*, where u_* is the friction velocity defined by $\tau_0 \equiv \rho u_*^2$, τ_0 being the surface shearing stress and ρ the air density.

If the potential density is independent of height (neutral hydrostatic stability) the velocity gradient is found to vary quite accurately as the inverse of the height measured from a reference plane near the top of the roughness elements and

$$\frac{dU}{dz} = \frac{u_*}{\kappa z}, \tag{17.1}$$

where κ is constant.

It is easy to see that (17.1) is a reasonable relation, though the "proofs" of it to be found in the literature are to be treated with caution. If, away from the surface, the turbulent motion is not affected by viscosity or other processes by which the stress is communicated to the surface, nor by the fact that the boundary layer is of finite thickness, but has its intensity and scale determined by the Reynolds stress and the height, then (17.1) follows on dimensional grounds. It is written in terms of dU/dz rather than U because a uniform translation can have no effect on the internal dynamics of the flow.

The profile of a transferable scalar such as potential temperature, specific humidity, or the concentration of

gases such as carbon dioxide can be treated similarly. Limiting the discussion again to neutral hydrostatic stability means that any variation in temperature or humidity must be small or combined in such a way as to maintain the potential density independent of height. As for momentum the vertical transfer by the turbulence will be governed by u_* and z: the potential temperature profile will be given by

$$\frac{d\Theta}{dz} = \frac{\theta_*}{\alpha_0 \kappa z}, \qquad (17.2)$$

where θ_* is a scale temperature defined by $u_* \theta_* \equiv \langle w\theta \rangle$, w being vertical velocity, and the constant α_0 is introduced to allow for the possibility that the transfer of a scalar quantity may differ from that of momentum.

In a similar way the humidity profile is given by

$$\frac{dQ}{dz} = \frac{q_*}{\alpha_0 \kappa z} \qquad (17.3)$$

with $u_* q_* \equiv \langle wq \rangle$. The same constant α_0 is used because it seems unlikely that different scalars will have different transfer properties in fully turbulent flow.

In (17.2) and (17.3), Θ is the mean temperature and Q the mean humidity, θ and q being the respective fluctuating quantities. The covariances $\langle w\theta \rangle$ and $\langle wq \rangle$ measure the heat flux H and the water vapor flux E as

$$H = c_p \rho \langle w\theta \rangle \quad \text{and} \quad E = \rho \langle wq \rangle$$

by analogy with the Reynolds stress $\tau = -\rho \langle wu \rangle$ (c_p is the specific heat at constant pressure, and u is the horizontal component of velocity).

It is perhaps surprising that the mean gradients are unaffected by the characteristics of the surface—one might expect the expressions for them to be valid only at heights large compared with some height typical of the surface geometry. But by choosing the zero plane suitably, often just below the tops of the surface-roughness elements, the formulas fit quite well down to heights only just above them.

17.2.2 Near-Surface Profiles in Nonneutral Conditions

It has been known for a long time that a vertical gradient of potential density can have a profound effect on turbulence (Richardson, 1920). When the density increases upward, so that the mean situation would be statically unstable, the mixing action of the turbulence produces a downward density flux, and buoyancy forces feed energy into the turbulence so as to augment the action of the windstress. So in unstable conditions, for a given value of the shear stress, the turbulence will be more vigorous and its ability to transfer heat and momentum greater than in neutral conditions. In stable conditions the converse is true.

How the buoyancy forces operate is only partly understood, although some theories based on the insertion of simple physical approximations into the Friedman-Keller equations for the variances and covariances of the velocity components and the density have had considerable success. It may be noted that since the work done by the buoyancy forces involves a product of their magnitude with the distance over which they operate, their effect is most pronounced on the large scales of motion. Hence one expects large eddies to be preferentially destroyed in stable conditions and preferentially sustained in unstable conditions: the scale of the most active part of the turbulence will be smaller in stable conditions than in unstable. Also, since the scale of the motion decreases as the surface is approached, so also does the effect of the buoyancy. It follows that sufficiently near the surface the active part of the motion is governed by the laws appropriate to neutral conditions.

In the surface layer great simplification has been achieved by the use of dimensional arguments to develop what is called "the similarity theory of the surface layer." It applies to the components of the motion that have scales smaller than the depth of the surface layer and so are generated and controlled within it. Recognizing that the fluxes of momentum and potential density are nearly independent of height in the surface layer, and that the mean gradients are unaffected by the detailed transfer processes at the boundary, Russian workers (Obukhov, 1946; Monin and Obukhov, 1954) were led to use the fluxes as key quantities in the surface layer. This was an imaginative development, at a time when fluxes were much harder to measure than mean gradients: it has provided a very useful means of systematizing many varied observations.

The assumption is made that turbulent quantities in the surface layer are unaffected by all quantities external to it, such as the total thickness of the boundary layer and detailed transfer processes at the surface. The basis of the theory is to use as the independent variables z, u_*, and δ_* (defined by $\delta_* u_* \equiv \langle \delta w \rangle$, where δ is the buoyancy fluctuation). All the properties of the turbulence are expressed in terms of them.

From these variables only one dimensionless group can be found. It is

$$\zeta = z/L, \quad \text{where} \quad L = u_*^2/\kappa \delta_* . \qquad (17.4)$$

L is called the Monin–Obukhov length after the originators of the theory. κ has been introduced because they included it in their initial definition.

It follows that all dimensionless properties of the turbulence must depend solely on ζ. In particular the dimensionless velocity profile will be a function of ζ alone,

H. Charnock

$$\frac{\kappa z}{u_*}\frac{dU}{dz} = \phi_M(\zeta),\qquad(17.5)$$

as will be the profile of a transferable scalar

$$\frac{\kappa z}{\theta_*}\frac{d\theta}{dz} = \phi_H(\zeta).\qquad(17.6)$$

17.2.3 Alternative Stability Parameters

The use of the Monin–Obukhov length has the disadvantage that it requires knowledge of the fluxes, which is not always available. It is sometimes more convenient to work with the gradient form of the Richardson number Ri, which is defined by

$$Ri = \frac{g}{\rho}\frac{d\rho}{dz}\Big/\left(\frac{dU}{dz}\right)^2,\qquad(17.7)$$

g being the acceleration due to gravity. According to the similarity theory Ri should be a universal function of ζ in the surface layer.

In his original paper Richardson (1920) showed that the rate per unit mass at which work had to be done by the turbulence against buoyancy forces was $\delta_* u_*$. He pointed out that the ratio of this to the rate at which the shear stress produced turbulent energy, $u_*^2(dU/dz)$, could not exceed unity unless energy was being brought into the region from outside. This ratio is now called the flux Richardson number, Rf, and is related to Ri, to ϕ_M, and to ζ by

$$Rf = \delta_*\Big/\left(u_*\frac{dU}{dz}\right) = \alpha Ri = \zeta/\phi_M,\qquad(17.8)$$

where $\alpha = \phi_M/\phi_H$ is itself a function of Ri or ζ.

It may be noted that only two empirical functions are needed to describe mean profiles and that the relations between the variables enable all the functions required in connection with mean profiles to be derived from whichever two functions can be conveniently measured.

17.2.4 Flux-Gradient Observations

To verify (17.1) for the mean-velocity profile in neutral conditions and to determine κ, it is necessary to measure the surface stress. From laboratory pipe measurements it was known that $\kappa \simeq 0.4$, and the measurements of Sheppard (1947), who simulated an area of ground surface and measured the forces on it with a spring balance, confirmed that the same value applied to the lower atmosphere. Later measurements using the drag-plate technique have given excellent results in suitable conditions.

A second method is to measure fluctuations of the horizontal u and vertical w components of the air flow. The turbulent stress is (nearly) $-\rho\langle uw\rangle$. It is necessary to use a fast-response instrument that responds to the whole range of frequencies contributing to the stress, and to have computer processing for the spectra, covariance, etc., but several workers have succeeded in producing consistent results. Such techniques can also be used, given measurement of fluctuating temperature and humidity, to estimate heat and water-vapor fluxes from $\langle w\theta\rangle$ and $\langle wq\rangle$.

Such rapid-response devices and analysis facilities can also be used to estimate the dissipation rates for turbulent energy, temperature variance, and humidity variance. In suitable conditions these can be related to the respective fluxes.

In spite of a good deal of work the value of κ is not universally agreed upon: this is partly due to the difficulty of allowing for fluctuations in the surface stress. When this is taken into account u_* in (17.1) should be replaced by its mean value $\langle(\tau/\rho)^{1/2}\rangle$, which is less than $\langle\tau/\rho\rangle^{1/2}$.

Pruitt, Morgan, and Laurence (1973) made careful measurements using a large drag plate to determine that $\kappa = 0.42$; allowing for a slight overestimate due to fluctuating stress it seems that the generally accepted value, $\kappa = 0.40$, is not far wrong.

There is not space here to deal adequately with the many observations that have been made, particularly over land, which have established the forms of ϕ_M and ϕ_H. They have been reviewed by Plate (1971), Monin and Yaglom (1965, 1967), and Högström (1974). According to Busch (1977), most atmospheric data are well represented by

$$\phi_M = \begin{cases} 1 + 5\zeta & (\zeta \geq 0) \\ (1 - 15\zeta)^{-1/4} & (\zeta \leq 0), \end{cases}$$

$$\frac{\phi_H}{\phi_H^{(0)}} = \frac{\phi_{OTS}}{\phi_0}\qquad(17.9)$$

$$= \begin{cases} 1 + 6\zeta & (\zeta \geq 0) \\ (1 - 9\zeta)^{-1/2} & (\zeta \leq 0), \end{cases}$$

where OTS means other transferable scalar. The value of $\phi_H^{(0)}$ ($= \alpha_0^{-1}$) values are scattered, but a reasonable value is 0.8.

There are some plausible arguments to support these forms but no satisfactory theory. Nevertheless it seems clear that the similarity theory of the surface layer provides an excellent framework in which to systematize observational studies of mean gradients and of turbulent fluctuating quantities in the surface layer. The basis of the theory is that such quantities are unaffected by the characteristics of the underlying surface, so the results so far given apply over both land and sea: the only requirement (by no means easy to satisfy) is that of uniformity in space and steadiness in time.

Previous expressions for profiles have been written in terms of gradients, like dU/dz, because by the hypotheses used a uniform translation can have no bearing on the internal structure of the flow. To integrate, so as to get an expression for, say, $U(z)$, requires a boundary condition within what can be called the *interfacial layer*, which includes the surface itself and the air above up to a height comparable to that of the elements that make up the surface. Processes in this layer are complicated and not well understood.

On integration of (17.1) we have for the wind profile in neutral conditions

$$\kappa \frac{U}{u_*} = \ln\left(\frac{z}{z_s}\right) \tag{17.10}$$

z_s is merely a constant of integration, whose value is determined by the surface geometry and surface processes. It has no influence on the internal dynamics of the flow.

Similarly, integration of (17.2) and (17.3) for the temperature and humidity profiles in neutral conditions gives

$$\alpha_0 \kappa (\Theta - \Theta_0) = \theta_* \ln(z/z_\theta), \tag{17.11}$$

$$\alpha_0 \kappa (Q_0 - Q) = q_* \ln(z/z_q) \tag{17.12}$$

where Θ_0, Q_0 are the potential temperature and the humidity at the surface and z_θ, z_q are constants of integration analogous to z_s. Like z_s they have no influence on the internal structure of the flow: changing them has the effect of adding a constant amount to the temperature and the humidity.

Turning to the more complicated expressions, (17.5) and (17.6), and integrating to get the profiles of velocity and potential temperature in nonneutral conditions we have

$$\kappa U/u_* = \int_{z_0}^{z} (\phi_M/z') \, dz'$$

$$= f_M(\zeta) + \phi_M(0) \ln(z/z_0)$$

where

$$f_M(\zeta) = \int_0^\zeta [(\phi_M - \phi_0)/\zeta'] \, d\zeta'. \tag{17.13}$$

The lower limit has been taken as zero instead of z_0/L since $z_0 \ll L$ and ϕ_M is assumed continuous at the origin.

Thus the departure from the neutral logarithmic form is given by f_M with ζ positive for stable, and negative for unstable conditions. All the stable profiles are similar to each other, as are all the unstable ones, the neutral profile being a limiting case.

Analogously,

$$\kappa(\Theta - \Theta_0)/\theta_* = f_H(\zeta) + \phi_H(0) \ln(z/z_\theta) \tag{17.14}$$

where

$$f_H(\zeta) = \int_0^\zeta [(\phi_H - \phi_H(0))/\zeta'] \, d\zeta'.$$

These rather formal results can be summarized by remarking that profiles like U/u_* are functions of ζ $(= z/L)$ and of z/z_0. The basic requirement of the similarity theory of the surface layer is that the internal dynamics of the flow is unaffected by the boundary processes so that

$$\kappa U/u_* = f(\zeta, z/z_0) = f_1(\zeta) + f_2(z/z_0)$$

$$= f_M(\zeta) + \ln(z/z_0).$$

The basic unknowns in the problem are those in the interfacial layer, represented by z_0, z_θ, z_q.

17.3.1 Transfer Coefficients over the Sea

So far as the relation between stress and velocity gradient is concerned, (17.1) indicates that the turbulence acts as an effective (eddy) viscosity of magnitude

$$K_M = \kappa u_* z.$$

This is usually much greater than the molecular viscosity ν, but below a height $\nu/\kappa u_*$ it is smaller, and molecular transfer will dominate the motion. If the surface is fairly smooth, so that the typical height of the roughness elements h_r is smaller than this, they will be submerged in the viscous layer and play little part in communicating stress to the surface. The flow is then said to be aerodynamically smooth (though in fact it is fully turbulent), and, since h_r is irrelevant, dimensional reasoning gives

$$u_* z_s/\nu = \text{constant} = 0.11 \quad \text{by observation.}$$

If, on the other hand, $h_r \gg \nu/\kappa u_*$, the stress is communicated to the surface by the form drag of the roughness elements. Then the molecular viscosity is irrelevant and

$$z_s = z_0,$$

where the so-called roughness length z_0 depends in a complicated way on the size, shape, and spacing of the roughness elements. There is no good theory for relating z_0 and h_r: typically for close-packed granular roughness elements $z_0 = h_r/30$.

In the intermediate case $h_r \simeq \nu/\kappa u_*$, z_s/h_r is a function of $u_* h_r/\nu$ that is known from laboratory observation.

A complication is that the wind can modify the geometry of the surface over which it blows. Long grass is flattened by the wind, and E. L. Deacon (1953) observed that z_0 for grass 700 mm long falls from 90 mm in light winds to less than 40 mm in strong winds. On the other hand, when particles from the surface are

carried into the air, as in blowing sand or snow, the value of z_0 is much larger than for the undisturbed surface.

The most important surface whose geometry is affected by the wind is the ocean. Its aerodynamic roughness has been the subject of much research over the last decades.

At very low wind speeds, before waves or ripples have been generated, the sea would be expected to behave as an aerodynamically smooth surface, and this is generally observed. When waves appear, the wind profile in neutral conditions remains closely logarithmic down to levels close to the surface, but the effective roughness length increases from the aerodynamically smooth value. From a series of careful wind-profile measurements over an artificial lake, and taking into account earlier observations, Charnock (1955) suggested that the aerodynamic roughness length was determined by the shearing stress, and used the simplest nondimensional relation

$$z_0 = \alpha_1 u_*^2/g. \qquad (17.15)$$

The same expression but with a different value for α_1 had been found by Ellison (1956) using observations reported by Hay (1955). The implication of such a formula is that, while z_0 depends in a complicated way on the waves generated, the wave structure in turn is determined by the stress on the surface. The coefficient α_1 is at most a weak function of the faster, and so of the larger, waves, with the possible implication that the stress is transmitted locally, and to the short waves and ripples. This raises the question why g is used in (17.15) rather than other properties of the fluid such as its viscosity or surface tension. Lengths can be formed using u_* and ν (as in aerodynamically smooth flow), and using the surface tension S and u_*: in both cases the lengths decrease as u_* increases, so it is not likely that z_0 depends on ν or S in any simple way. But the fluid mechanics of the wavy surface is complicated and no adequate theory exists.

The usefulness of (17.15) is tested by observation, and here there has been considerable difference of opinion. Observations of the surface stress over the sea have been made by numerous workers, using various methods. The most common methods have been the use of the wind profile and eddy correlation. Most workers have preferred to express their results in terms of a drag coefficient C_D given by

$$\tau_0 = C_D(10)\rho U_{10}^2$$

the 10 being inserted as a reminder that the value of C_D depends on the height at which U is measured: 10 m is commonly used. U_{10}, and so $C_D(10)$, is also affected by the static stability, but this can be allowed for using similarity theory:

$$C_D = \frac{C_{DN}}{[1 + \kappa^{-1}C_{DN}^{1/2}f_M(\zeta)]^2} \, ,$$

where f_M is given by (17.13) and

$$C_{DN} = \frac{\kappa^2}{(\ln z/z_0)^2}$$

is the neutral drag coefficient.

Garratt (1977) has recently made a thorough review of previously reported values of C_{DN} in relation to U_{10}. Until about 1970 the values were scattered (though less so than they were 20 years before—see Charnock, 1951). They are shown in figure 17.1 and table 17.1. Since 1970 many more observations have been reported, using better methods, and Garratt has estimated C_{DN} from the 17 publications listed in table 17.2, excluding some, for reasons detailed in his paper. The resulting values are plotted in figure 17.2, in which reasonable agreement with (17.15) is shown, though the considerable scatter increases at wind speed greater than 15 m s^{-1}.

Some authors have estimated the surface stress in hurricanes by integrating the ageostrophic wind component. These are given in table 17.3 and figure 17.3 (again due to Garratt, 1977): there is some indication that (17.15) is satisfied in winds up to 50 m s^{-1}. Garratt gives $\alpha_1 = 0.0144$ as an acceptable value.

It seems from Garratt's review that (17.15) is sufficient for many purposes. But its physical basis is still very unsatisfactory: the implied roughness lengths are small ($\sim 10^{-1}$ mm), and we have no clear idea as to how they are determined. That the high-wavenumber range of the wave spectrum is involved seems probable, and is supported by experiments using surface films and detergents that eliminate short waves and much reduce the drag for a given wind.

Our knowledge of z_θ, z_q, and the physical properties on which they depend is even less satisfactory. Owen and Thompson (1963) have put forward a theoretical framework that allows comparisons between measurements of heat and of vapor transports from fixed rough surfaces. They give a formula that, assuming α_0 [equation (17.3)] to be 1.3, becomes

$$\ln(z_0/z_\theta) = 2.0Pr^{0.75}(u_*z_0/\nu)^{0.33}, \qquad (17.16)$$

though the numbers are tentative. $Pr = \nu/\nu_T$ where ν_T is the kinematic molecular diffusivity for the property being transferred. Fortunately u_*z_0/ν is small over the ocean so $z_0 \simeq z_\theta$ is a reasonable approximation. But if a formula like (17.16) does apply, and if z_0 is given by (17.15), then z_θ will gradually become less than z_0 as u_* increases. Kitaigorodskii (1970) gives a critical review of existing observations, as do Friehe and Schmitt (1976) and Busch (1977), but the experimental scatter makes it difficult to generalize.

Table 17.1 Main Reviews of the Neutral Drag Coefficient over the Sea[a]

Source	Wind speed range $(\mathrm{m\,s^{-1}})$	$C_{DN}(10)$ $(\times 10^3)$	Variability $(\%)$	Number of references
A. Priestley (1951)	2.5–12 strong	1.25[b] 2.6[c]	?	Not stated
B. Wilson (1960)	~1–5 9–20	1.42 2.37	±50 } ±25 }	47
C. Deacon and Webb (1962)	2.5–13	$1 + 0.07\,V$	±25–50	9
D. Robinson (1966)	3–8.5 2.5–14	1.8[d] 1.48[e]	±30 } ±15 }	14
E. Wu (1969b)	3–15 15–21	$0.5\,V^{0.5}$ }[f] 2.5 }	±30 } ±10 }	30
F. Hidy (1972)	2–10	1.5	±30	8

a. Showing wind speed range, best estimate of $C_{DN}(10)$ (either as a constant or a function of wind speed), and typical data variability as a percentage of $C_{DN}(10)$ value over the wind speed range considered (see figure 17.1). [After Garratt (1977), who summarized the reviews.]
b. Actually based on Deacon (1950): *Nature* 165, p. 173.
c. Quotes Sverdrup et al. (1942) and Munk (1947).
d. Micrometeorological data.
e. Geostrophic departure.
f. Overall variation close to Charnock relation with $\alpha = 0.016$.
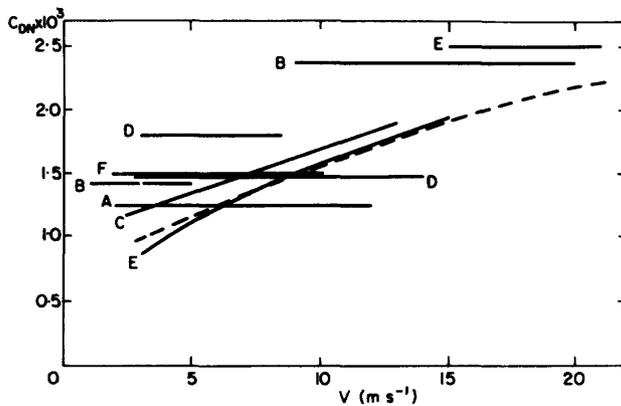
Figure 17.1 Mean curves of $C_{DN}(10)$ plotted against V (10 m) for review sources shown in table 17.1. Dashed curve is based on $z_0 = \alpha u_*^2/g$ with $\alpha = 0.016$ and $\kappa = 0.41$.(Garratt, 1977.)
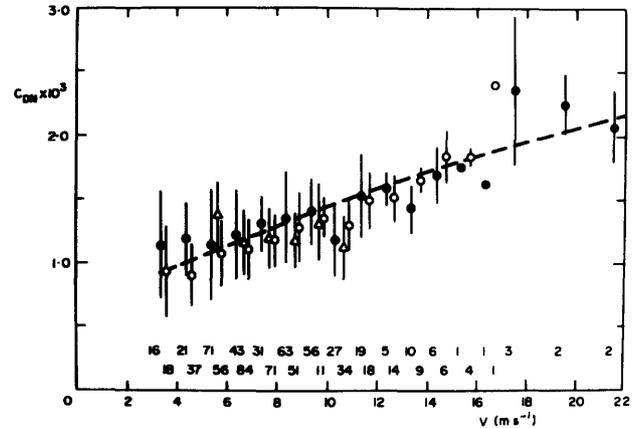
Figure 17.2 Neutral drag coefficient values as a function of wind speed at 10-m height, based on individual data taken from the recent literature (see table 17.2 and Garratt, 1977). Mean values are shown for 1-m·s⁻¹ intervals based on the eddy correlation method (●) and wind profile method (O); Hoeber's wind profile data are also shown (△). Vertical bars refer to the standard deviation of individual data for each mean, with the number of data used in each 1-m·s⁻¹ interval shown above the abscissa axis: top line refers to (●), bottom line to (O). The dashed curve represents the variation of $C_{DN}(10)$ with V based on $z_0 = \alpha u_*^2/g$ with $\alpha = 0.0144$. (Garratt, 1977.)

Table 17.2 Neutral Drag Coefficient Values over the Ocean[a]

Source	Wind speed range (m s^{-1})	$C_{DN}(10)$ $(\times 10^3)$	Variability σ (%)	Number of data (n)	Method	Platform	Comments
1. Smith and Banke (1975)	2.5–21	$0.63+0.066V$	30	111	ec	Mast	Also utilizes data of Smith (1973) using thrust and sonic anemometers
2. Kondo (1975)	3–16	$1.2+0.025V$	15	—	waves	Tower	Utilizes data on wave amplitudes from Kondo et al. (1973)
3. Davidson (1974)	6–11.5	1.44	?	114	ec	Large buoy	Does not correct for stability effects
4. Wieringa (1974)	4.5–15	$0.62V^{0.37}$ or $0.86+0.058V$	20	126	ec	Tower	Surface tilt and wp estimates are excluded
5. Kitaigorodskii et al. (1973)	3–11	0.9 (at 3 m s^{-1}) to 1.6 (at 11 m s^{-1})	?	29	ec	Tower	Plots C_{DN} as a function of $u_* z_0/\nu$
6. Hicks (1972)	4–10	$0.5V^{0.5}$	25	74	ec	Tower	Accepts C_{DN} relation as same as Wu (1969b)
7. Paulson et al. (1972)	2–8	1.32	25	19	wp	Large buoy	Uses $\kappa = 0.40$
8. Sheppard et al. (1972)	2.5–16	$0.36+0.1V$	20	233	wp	Tower	Uses $\kappa = 0.40$
9. De Leonibus (1971)	4.5–14	1.14	30	78	ec	Tower	
10. Pond et al. (1971)	4–8	1.52	20	20	ec	Large buoy	
11. Brocks and Krügermeyer (1972)	3–13	$1.18+0.016V$	15	152	wp	Buoy	Data from North Sea and Baltic Sea—uses $\kappa = 0.40$
12. Hasse (1970)	3–11	1.21	20	18	ec	Buoy	See text on data interpretation
13. Miyake et al. (1970)	a. 4–9	1.09	20	8	ec	Mast	See text on data interpretation—uses $\kappa = 0.40$
	b. 4–9	1.13	20	8	wp	Mast	
14. Ruggles (1970)	2.5–10	1.6	50	276	wp	Mast	C_D anomalies found at a number of wind speeds—uses $\kappa = 0.42$
15. Hoeber (1969)	3.5–12	1.23	20	787	wp	Buoy	Data from equatorial Atlantic—uses $\kappa = 0.40$
16. Weiler and Burling (1967)	a. 2–10.5	1.31	30	10	ec	Mast	
	b. 2.5–4.5	0.90	75	6	wp	Mast	Uses $\kappa = 0.40$
17. Zubkovskii and Kravchenko (1967)	3–9	$0.72+0.12V$	15	43	ec	Buoy	wp estimates of u_* show low correlation with ec; possible effect of buoy motion

a. Taken from the recent literature for a reference height of 10 m: ec = eddy correlation method; wp = wind profile method. σ is the standard deviation of n data points about the mean value. [After Garratt (1977), who compiled and evaluated the source material.]

Table 17.3 Neutral Drag Coefficients over the Ocean[a]

Source	Wind speed range $(\mathrm{m\ s^{-1}})$	$C_{\mathrm{DN}}(10)$ range $(\times 10^3)$	Comments
A. Miller (1964)	17–52	1.0–4.0 (linear)	Hurricanes Donna and Helene— ageostrophic
B. Hawkins and Rubsam (1968)	23–41	1.2–3.6 (discontinuous)	Hurricane Hilda— ageostrophic
C. Riehl and Malkus (1961)	15–34	2.5	Held constant to achieve angular momentum balance
D. Palmén and Riehl (1957)	5.5–26	1.1–2.1 (linear)	Composite Hurricane data—ageostrophic
E. Kunishi and Imasoto (see Kondo, 1975)	14–47.5	1.5–3.5	Wind flume experiment
F. Ching (1975)	7.5–9.5	1.5	Vorticity and mass budget at BOMEX

a. Taken from the literature, for hurricane and vorticity-mass-budget data analyses. Also included are wind flume data of Kunishi and Imasoto (see Kondo, 1975). [After Garratt (1977), who compiled and evaluated the source material.]
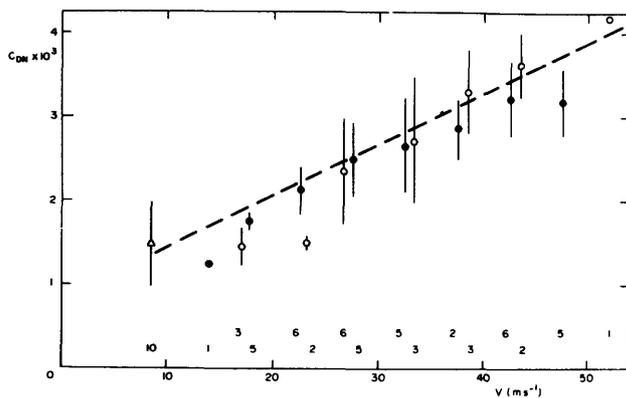
Figure 17.3 Mean values of the neutral drag coefficient as a function of wind speed at 10-m height for 5-m-s^{-1} intervals, based on individual data from hurricane studies (O), wind flume experiment (●), and vorticity mass budget analysis (△)—see table 17.3. Vertical bars as in figure 17.2. The number of data contained in each mean is shown below each mean value, and immediately above the abscissa scale. The dashed curve represents the variation of $C_{\mathrm{DN}}(10)$ with V based on $z_0 = \alpha u_*^2/g$ with $\alpha = 0.0144$. (Garratt, 1977.)

Although our knowledge of the complicated processes in the interfacial layer is very unsatisfactory, we can, by using similarity theory and empirical knowledge of z_0, z_θ, etc., derive formulas from which the surface fluxes can be estimated from ships' observations in the near-surface layer of, say, temperature, humidity, and wind speed at a known height, together with sea-surface temperature. The errors in such estimates will be considerable, but they are more likely to be due to the errors in the ships' observations than to deficiencies in the formulas.

Calculations of the fluxes from climatological data [Jacobs (1951), Privett (1960), Budyko (1956), and more recent work by Bunker (1976) and Saunders (1977)] are of great value even though their accuracy is limited by the low precision of the ships' observations and by lack of uniformity of their cover of the ocean. They are thought unlikely to provide estimates from which the poleward heat transport by the ocean can be deduced, but will be useful in attempts to interpret the work of Oort and Vonder Haar (1976).

17.4 Waves

The most obvious effect of the wind on the sea is the generation of waves. They have been much studied, for there is no doubt of their economic importance: the design of ships, of harbors, and of sea defenses all need estimates of the waves to be encountered, to say nothing of the questions raised by the reflection of sound and light at the sea surface.

What is less obvious is how they fit into the coupled mechanics of the ocean and the atmosphere—how the winds and currents would differ if by some magic device the surface waves were eliminated. The drag coef-

H. Charnock

ficient for surface friction seems to be largely independent of the larger waves, as do the exchange coefficients for heat and water vapor. The transfers of energy and momentum from the atmosphere to waves on the ocean have been studied extensively: considerable progress has been made but there is still no complete agreement about the complicated fluid mechanics involved.

The wartime work, well confirmed and extended by Snodgrass and his colleagues (1966), established the basic fact that swell traveled thousands of kilometers, at the theoretical group velocity, without much attenuation. This implied that waves did not interact strongly with each other, or with ocean currents, so that a Fourier spectral representation was physically appropriate as well as mathematically convenient. From it one can derive all the statistical distributions of the waves for which the model is valid (Longuet-Higgins, 1962). From a practical point of view we must learn how to recognize and circumvent the limitations imposed by nonuniformity of the wind structure, and how to predict the evolving (directional) wave spectrum from such meteorological observations as are available, or from the output of computer simulations.

17.4.1 The Fetch-Limited Case

An important but relatively easily realizable case is that of a steady wind blowing off a straight shore, so that the duration of the wind is irrelevant and the fetch is well defined. An early contribution to this problem came from Burling (1959), who measured wave spectra at short fetches on an artificial lake using a newly developed capacitance-wire wave recorder.

In this case one can hope that the energy of the waves at a given fetch will be proportional to the work done by the wind on the water. If this is crudely estimated as proportional to the shearing stress times a distance measured by the fetch, then

$$\zeta = \text{constant} \times u_*(X/g)^{1/2} \tag{17.17}$$

where ζ^2 is the mean square wave amplitude, and X the fetch.

Burling's results supported the simple relation (Charnock, 1958b) and it was confirmed for longer fetch by the results of the JONSWAP experiment (Hasselmann and colleagues, 1973). The Joint North Sea Wave Project (JONSWAP) was an important cooperative venture in which a group of scientists from several countries pooled their observational resources to obtain wave spectral data good enough to allow generalization about its evolution with varying wind and fetch. They used a linear array of wave sensors spaced along a 160-m profile extending westward from the island of Sylt in the North Sea (figure 17.6).

As regards the wave energy the JONSWAP data supported (17.17). Figure 17.4, from Phillips (1977a), shows Burling's observations together with those of JONSWAP: it is plotted in terms of nondimensional coordinates proposed by Kitaigorodskii (1962) to show that the constant of (17.17) is about 1.26×10^{-2}.

Burling was also able to calculate spectra. The photographic recording technique and the analogue spectral analyzer then in use much increased the effort needed, while restricting the precision of the estimates. Nevertheless Burling was able to establish the main features of the nondirectional frequency spectrum. He found that there was a very rapid increase, at low frequencies, to a maximum value at frequency n_0 determined by the wind speed and the fetch. At frequencies greater than n_0 the spectra fell off, approximately as $(\text{frequency})^{-5}$. In this so-called equilibrium range of the spectrum the energy was largely independent of both wind and fetch. Figure 17.5, from Phillips (1977a), includes some of Burling's spectra together with those of later workers.

Those of the JONSWAP project are broadly similar (figure 17.6), but near the peak frequency they show an overshoot which had first been observed by Kinsman (1960) and by Barnett and Wilkerson (1967), who used an airborne radar altimeter to measure one-dimensional wavenumber spectra over larger fetches. Snyder and Cox (1966) had measured the evolution of one particular spectral band (around 0.3 Hz) by towing an array of wave recorders downwind at the appropriate group velocity, finding that the energy "overshot," in
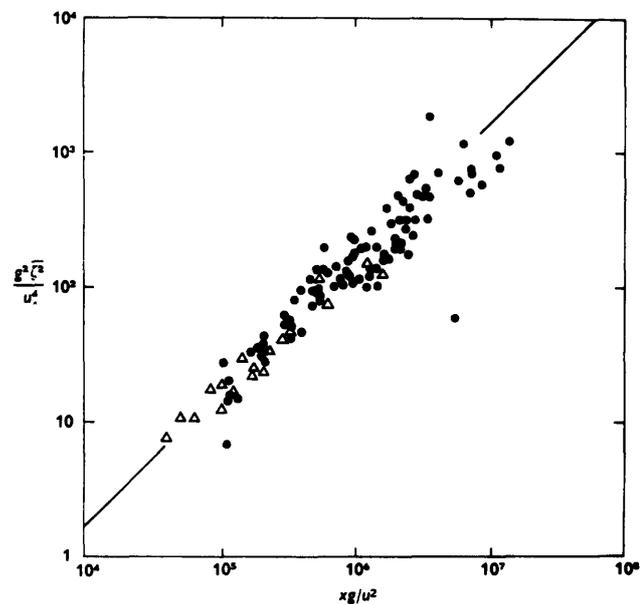
Figure 17.4 Field measurements of the dimensionless mean-square surface displacement $g^2\overline{\zeta^2}/u_*^4$ as a function of dimensionless fetch Xg/u_*^2. Data points are represented thus: Hasselmann et al. (1973), ●; Burling (1959), △. The line in the background is $g^2\overline{\zeta^2}/u_*^4 = 1.6 \times 10^{-4}Xg/u_*^2$. (Phillips, 1977a.)
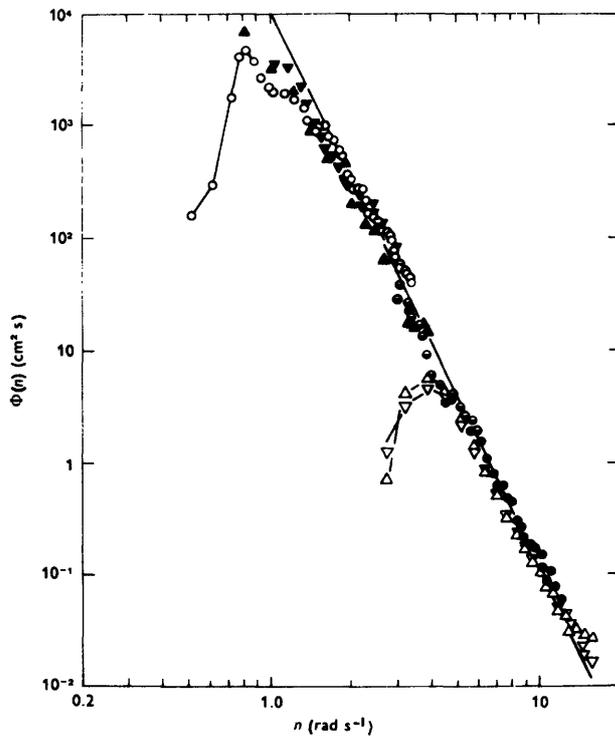
Figure 17.5 The equilibrium range of the frequency spectrum of wind-generated waves. The logarithmic vertical scale covers six decades. The shape of the spectral peak is included in only three cases; otherwise only the saturated part of each spectrum is shown. Key to measurements:

O	Stereo-Wave Observation Project (Pierson, 1960)	floating wave spar	1 spectrum
▲	Longuet-Higgins et al. (1963)	accelerometer	1 spectrum
▼	DeLeonibus (1963)	inverted fathometer	Mean of 6 spectra
△	Kinsman (1960) November series	capacitance probe	Mean of 16
▽	Kinsman (1960) July series	capacitance probe	Mean of 16
●	Burling (1959)	capacitance probe	Mean of 11
⊖	Walden (1963)	probe and cinematograph	1 spectrum

[After Phillips (1977a), who compiled and plotted the original observations.]

that it grew faster than would be expected, for the spectrum as a whole, from linear theory.

The frequency of the spectral peak is clearly an important descriptor of the wave field. Its value for Burling's, the JONSWAP, and other observations is shown in figure 17.7 (from Phillips 1977a). The values are again plotted in the nondimensional form suggested by Kitaigorodskii. It is perhaps worth noting that if L_0, the wavelength at the spectral peak, be given by $L_0 n_0^2 = 2\pi g$, then

$$L_0 = 1.3 u_*\{X/g\}^{1/2}$$

$$\approx 100\zeta, \tag{17.18}$$

consistent with the bulk of the energy being in the equilibrium n^{-5} range.

As a result of the many observations of waves we now have reasonably clear information on the evolution of the surface wave field in deep water, at least so far as the frequency spectrum is concerned. Directional spectra are more difficult to measure and information is correspondingly sparse.

17.4.2 The Energy and Momentum Balance of the Wave Spectra

The main purpose of the JONSWAP project was to determine the source function in the spectral equation for the energy balance

$$\frac{\partial E}{\partial t} + v_{gi}\frac{\partial E}{\partial x_i} = S. \tag{17.19}$$

E is the wave energy and v_{gi} the component of the appropriately generalized group velocity in the direction of coordinate x_i. The basic result is shown schematically in figure 17.8, where the source function S is seen to have a characteristic positive–negative shape.

The source function at a particular frequency is made up of three components—the energy transferred to the waves by the wind, the energy dissipated, and the energy transferred from other regions of the spectrum.

The spectral representation used is based on a superposition of sinusoidal waves traveling independently. But the hydrodynamic equations are nonlinear and the linear approximation is only valid when the wave slope is small, i.e., when the accelerations are small relative to the acceleration of gravity.

To treat the nonlinear terms, one substitutes the linear solution into the nonlinear terms, to get a second-order solution with terms in the wave slope. Higher-order solutions have terms in (slope)², (slope)³, and so on. The primary waves are sinusoidal and the second approximation has sharper crests and flatter troughs. One gets terms involving products of pairs of primary waves, which produce secondary waves at their sum and difference frequencies.

H. Charnock
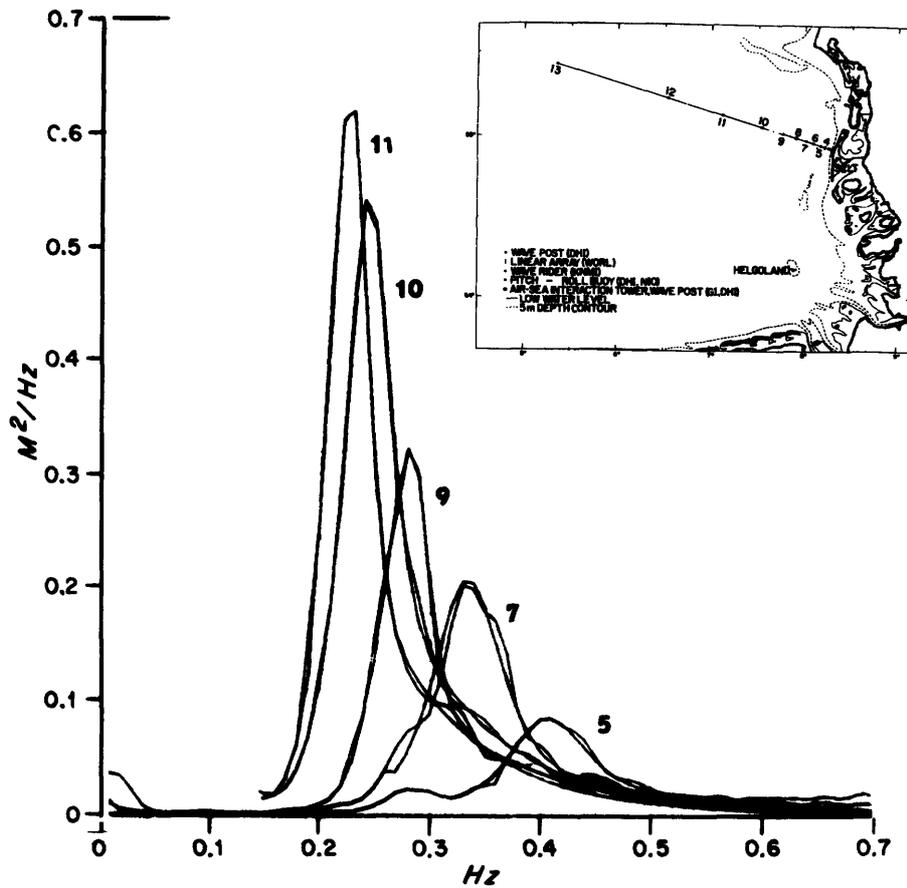
Figure 17.6 Evolution of wave spectrum with fetch for off-shore winds 11ʰ-12ʰ Sept. 15, 1968. Numbers refer to stations inset. (Hasselmann et al., 1973.)
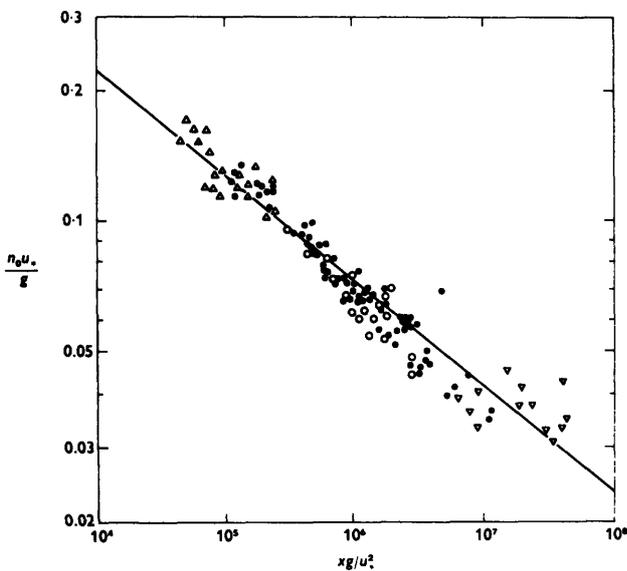
Figure 17.7 Field measurements of the dimensionless frequency of the spectral peak $n_0 u_*/g$ vs. dimensionless fetch Xg/u_*^2. Data points are as follows: Hasselmann et al. (1973), ●; Kitaigorodskii and Strekalov (1962), ∇; Mitsuyasu (1966), ○; and Burling (1959), △. The straight line in the background is $(n_0 u_*/g) = 2.2(Xg/u_*^2)^{-1/4}$. [After Phillips (1977a), who compiled and plotted the original observations.]

ENERGY BALANCE

S_{in} = Input from Atmosphere

S_{nl} = Nonlinear Wave-Wave Transfer

S_{ds} = Dissipation

Net Transfer $S = S_{in} + S_{nl} + S_{ds}$
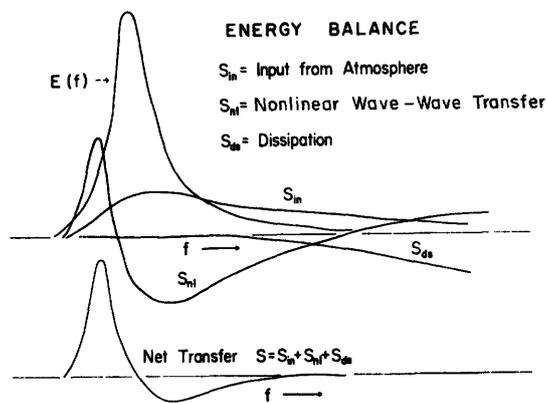
Figure 17.8 Schematic energy balance for the case of negligible dissipation in the main part of the spectrum. (Hasselmann et al., 1973.)

493
Air–Sea Interaction

The solution stays bounded provided there is no combination of

$$\mathbf{k}_3 = \mathbf{k}_1 \pm \mathbf{k}_2 \quad \text{and} \quad n_3 = n_1 \pm n_2$$

such that

$$gk_3 = n_3^2.$$

O. M. Phillips (1963) showed that no such combination occurs in surface gravity waves. But for tertiary waves he found that for

$$\mathbf{k}_4 = \mathbf{k}_1 \pm \mathbf{k}_2 \pm \mathbf{k}_3,$$
$$n_4 = n_1 \pm n_2 \pm n_3 \tag{17.20}$$

there exist combinations for which $gk_4 = n_4^2$, so there is a resonance, with energy being transferred from three primary waves to a new wave whose energy grows linearly with time. The interactions are weak, so it grows slowly, its time scale being of order (slope)[4] times a typical wave period. Such nonlinear interactions have been observed in careful laboratory experiments and shown to be consistent with the slow attenuation of ocean swell.

Hasselmann (1966) has exploited the analogy with collisions in high-energy physics, and he uses Feynman diagrams to represent nonlinear interactions, with wavenumber corresponding to momentum and frequency to energy. He has also given a complicated equation by which the nonlinear transfers can be calculated. Using an interaction equation derived by Longuet-Higgins (1976), Fox (1976, 1978) has given a simpler method applicable when the spectrum is narrow. Broader spectra have been studied by Webb (1978).

For the JONSWAP case S_{nl}, the contribution of nonlinear transfer is shown on figure 17.8. It has the same positive–negative shape as S and provides a reasonable qualitative explanation of the way in which the spectral peak goes to lower frequencies as the nondimensional fetch increases.

The contribution of S_{nl}, due to nonlinear weak interactions, is to redistribute wave energy within the spectrum. It is the best known of the terms that make up S:

$$S = S_{in} + S_{nl} + S_{ds} \tag{17.21}$$

where S_{in} represents the energy input from the atmosphere and S_{ds} the dissipation. Assuming the dissipation to be small in the energetic low-frequency band of the spectrum, the JONSWAP results indicate a schematic energy balance as in figure 17.8. Then the energy input has a distribution like that of the spectrum itself, as if the wave generation depends linearly on the spectrum, and the dissipation occurs mainly at high frequencies.

Attempts to calculate S_{in} theoretically have so far been unsuccessful. It involves the calculation of the covariances between fluctuations in the surface stress (both normal and tangential) and in the surface velocity. Phillips (1957) showed that turbulent pressure fluctuations in the natural wind would amplify waves traveling at the right convection velocity by a resonance mechanism. Like an earlier theory of Eckart (1953), the theory was qualitatively correct but the amplitude of atmospheric pressure fluctuations (rms pressure fluctuation $\simeq \tau_0$) was too small to produce waves of the amplitude observed. Miles (1957, 1959) calculated fluctuations induced by the mean wind blowing over the wavy surface: since the pressure fluctuations depend on the wave amplitude, the latter grows exponentially, but again the predicted growth rate was much less than that observed. Miles had been obliged to neglect the atmospheric turbulence in the interfacial layer, however, and nobody has yet succeeded in satisfactorily incorporating it. The problem was carefully discussed by Davis (1972), who used several different closure approximations, which gave variable results. He also found that the rate of energy transfer to the waves is critically dependent on the profile of mean flow very close to the interface. Gent and Taylor (1976), who have done numerical simulations of airflow over waves, avoided the problem by assuming that the surface has an assigned roughness, either constant or distributed along a long wave. Their solutions are more encouraging but the problem of calculating energy and momentum transfer in the interfacial layer is by no means solved.

Detailed observation of energy and momentum transfer in the interfacial layer also presents great difficulty. Since the drag coefficient of the sea surface is greater, but not very much greater, than that of an aerodynamically smooth surface, one might expect some direct viscous transfer. In this case the tangential stress must be supported, just below the interface, by a thin layer with strong shear. Equally, since the sea surface becomes increasingly rough, relative to an aerodynamically smooth surface, as the wind speed increases, there must be a good deal of momentum transport to irrotational or quasi-irrotational waves by pressure fluctuations. This was the basis of Jeffreys's (1925) theory. Valiant attempts have been made to measure pressure fluctuations relative to the wave profile by Dobson (1971), Elliott (1972), and Snyder (1974).

Such observations are extremely difficult. The static pressure fluctuations $O(\tau_0)$ are small, very small relative to the dynamic pressures in the airflow. To compute the energy and momentum transfer to the waves, the pressure is needed at the (moving) surface: this needs an extrapolation from a recorder as near the surface as possible, or a surface-following device, which introduces other problems. It is hardly surprising that the early results were not entirely consistent: roughly speaking Dobson's values gave the biggest growth

H. Charnock

rates, Elliott's were smaller (roughly $\frac{1}{2}$) and Snyder's even less.

These three authors have recently collaborated with Long in a field program in the Bight of Abaco in the Bahamas (Snyder, Dobson, Elliott, and Long, 1980). Preliminary results indicate that momentum transfer to the wave extends from the peak frequency to at least twice the peak frequency with little noticeable falloff. Observations at higher frequency will be necessary to allow an estimate of the total momentum transfer, but it seems clear that for the JONSWAP spectrum a significant fraction of the momentum first goes into waves; about 10% at long fetch ($gX/U_{10}^2 = 10^5$), rising to about 100% at shorter fetch ($gX/U_{10}^2 = 10^2$). There remains a need for critical observations at short fetch, but the high-frequency response that will be needed will be hard to achieve.

The dynamics of a near-surface viscous shear layer are also relevant: Banner and Phillips (1974) have shown that the speed of such a layer will be increased near the crest of a longer wave, so leading shorter waves to break. Such breaking may be made visible by dimples or pockmarks on the surface, particularly in the early development of a wave field. Banner and Melville (1976) have demonstrated that wave breaking, even on a small scale, is accompanied by separation of the airflow from the surface. This has strong implications both for momentum transfer and for the exchange of heat or water vapor. That the drag and analogous coefficients are small may prove to be due to the sporadic nature of the breaking process. The problem deserves further investigation since breaking waves seem to provide a limit between the spectrum of the longer Gaussian waves and the shorter nonlinear ripples: breaking waves on the open sea have been much neglected (Charnock, 1958a).

Another important phenomenon associated with breaking waves, with which one hopes more progress will be made in the next 20 years than in the last, is dissipation. It now seems more likely that breaking waves are more important than viscosity in dissipation, and Longuet-Higgins (1969a) has given an interesting calculation that implies that the proportion of wave energy lost per mean cycle is about 10^{-4}.

Measurements of mean and fluctuating velocities in waves are technically difficult, but there is growing evidence that the orbital velocities of the larger waves are inactive, in the sense that they provide variance but are so uncorrelated as to be inactive in the transfer of momentum. Jones and Kenney (1977) have argued that the near-surface layer in the water has many of the characteristics of the surface layer in the air, with scaling on u_* and z_0. Observations by Donelan (1978) show that as well as the wave orbital velocities there are fluctuations at lower frequency (possibly due to the shear in the mean profile) and at higher frequency

(possibly due to whitecapping). The momentum flux was entirely due to the low-frequency fluctuations. His general picture of the effects of wave breaking is that the wind stress produces a strongly sheared current near the surface, so that when a wave breaks the downward pulse of fluid produces a downward momentum transfer. Though each pulse of momentum is short, the intermittent nature of the phenomenon is reflected in the momentum flux at lower frequencies. The effect of whitecapping on the spectrum has been considered theoretically by Hasselmann (1974) as a strong interaction that is weak in the mean: because it is sporadic and local in physical space the energy loss is spread over much of the spectrum.

17.4.3 Langmuir Circulations

Another near-surface phenomenon that may be important in momentum transfer is the Langmuir cell. Langmuir cells are alternate left-handed and right-handed vortices in the vertical plane (horizontal rolls), aligned along the wind with surface velocities strongest in the convergence zones. It is easy to see that the stronger horizontal velocity there could combine with the sinking motion under the convergence zone to give mean stresses of the same order as the wind stress at the surface.

There have been many observations since Langmuir's (1938) first description, all supporting the cellular structure he found. Row spacings, often marked by streaks on the surface, are variable, typically 10 m in lakes and 100 m over the ocean: the surface current moves at about 10 cm s^{-1} faster in the streak than outside it. The vertical structure is less well known. An account of the observations is given by Pollard (1977); he also gives an account of theoretical attempts to explain these cells, from which it seems clear that complicated interactions in the surface wave field are involved. Faller (see chapter 16) has shown in laboratory observations that both wind and waves are necessary for the generation of Langmuir cells: it is thought that the vorticity of the shear flow produced by the wind stress is transformed by nonlinear interaction with crossing wave trains into the vorticity of the helices. The details are complicated but it seems likely that the Langmuir cells may represent a mechanism by which wave energy is converted to organized convection and to turbulence, which in turn may act to deepen the mixed layer.

17.5 The Atmospheric Boundary Layer

From a practical point of view the mean fluxes at the sea surface can now be calculated to acceptable accuracy from observations in the surface layer. The related characteristics of the surface wave field are also rea-

sonably well known and it can be assumed, with somewhat less confidence, that the momentum transferred from the atmosphere to the sea surface is then transferred to the ocean at the same place and time.

In all these cases our knowledge is empirical and there is a need for more understanding, leading to theoretical descriptions of the physical processes involved. But from an engineering viewpoint what was once thought of as the central problem of air–sea interaction has been reduced to some sort of order.

Problems change, however, and those of air–sea interaction are now of much greater scope. The recently renewed interest in climate and climatic change has led to a wider appreciation of the importance of the interaction between the atmosphere, the ocean, and characteristics of solid surfaces such as ice. Because almost all the energy for the motion comes from the sun it is conceptually attractive to regard the basic circulation of the atmosphere and ocean as the free convective response of the coupled system to solar heating. Air–sea interaction can now be taken to include all the problems of meteorology and oceanography.

Nevertheless the different physical properties of air and water, especially their relative opacities to electromagnetic radiation, lead to considerable decoupling: the mismatch is such that it is usually more rewarding to treat them separately, isolating topics like the effect of wind on the sea, or the effect of evaporation on the atmosphere. The darkness of the ocean has also made observations difficult, so less is known of its structure than that of the relatively transparent atmosphere.

No one disputes that the fluxes of heat, water vapor, and momentum that enter the atmosphere through its lower boundary layer are of crucial importance to the development of atmospheric flow patterns and weather on time scales ranging from minutes to months. There is no reason to doubt that they are equally important for longer-period climatic changes, but we know little of the degree of accuracy and detail in which they must be described for specific purposes, in particular for forecasting using computer models of the atmosphere, the ocean, or the coupled system.

Some suggestion that rather precise knowledge of the exchange processes will be needed comes from the relations that have been found (Namias, 1969; Bjerknes, 1969; Ratcliffe and Murray, 1970) between sea-surface temperature anomalies and subsequent weather patterns, though a direct causal connection has not been unambiguously demonstrated. To achieve such precision an understanding of the physical processes involved seems essential: attempts to use parameters without physical understanding may yield rapid progress in the early stages but seem likely to be inadequate in the long run.

At any given time atmospheric and oceanic motions on scales greater than 100 km or so can be treated as essentially inviscid and adiabatic, but there are localized regions where condensation processes, or the transport of heat, water, salt, or momentum by small-scale turbulence are important, even dominant. Examples of such regions are towering clouds, or groups of clouds, fronts, and the turbulent boundary layers near the earth's surface. For the present purpose it has seemed sensible and convenient to restrict the scope of air–sea interaction to studies of the mechanics and structure of the near-surface boundary layers of the atmosphere and the ocean.

For many years, as has been indicated, the subject was more restricted, essentially to the lowest 10 to 100 m of the atmosphere above the sea. This came about mainly because the routine observations available were those from ships. There were a few upper-air observations from weather ships, but their purpose was to map meteorological fields in the troposphere and lower stratosphere: exchanges with the ocean were not allowed for in routine forecasting.

Routine observations of the whole atmospheric boundary layer over the sea are still virtually nonexistent, the number of weather ships having decreased in recent years. What has developed rapidly is the numerical simulation of atmospheric processes, now used routinely as a basis for weather forecasting: when these are used to forecast for more than a day or so it begins to be necessary to include boundary-layer effects. Some models use many layers in an attempt to resolve the vertical structure of the boundary layer, ultimately relating fluxes to conditions in the surface layer, but the need to simulate small-scale turbulence in the boundary layer makes such a system prohibitively expensive in computer time unless the equations are drastically simplified. It seems more realistic to admit that the boundary layer has a different physics from most of the atmosphere above it and to seek to treat it as a whole. Then the height of the top of the atmospheric boundary layer is calculated explicitly and becomes the effective lower boundary of the largely frictionless atmosphere above. Such a method was adumbrated by Charnock and Ellison (1967) and has been developed by Deardorff (1972) and implemented by Arakawa (1975). The structure of the atmospheric boundary layer is now being increasingly studied, but it is much more complicated than the surface layer. It is not well mapped, nor are the physical processes that maintain it well understood.

The top of the atmospheric boundary layer is usually most obvious from inspection of the density variation with height, particularly over land in summer. Then a weakly stable condition is established during the night that is transformed after dawn by solar heating to a convective boundary layer at the surface. This is suf-

ficiently well mixed to have effectively constant potential temperature, and it deepens as it warms in accordance with the classical ideas of Gold (1933). It is easy to check that there is reasonable quantitative agreement between the available solar energy and the rate of warming of the boundary layer. That the level of turbulence inside such a convective boundary layer is much greater than in the free air above is obvious to anyone who has done much flying, but of course it can be confirmed instrumentally. It is also common to find that smoke or other pollutants are fairly uniformly mixed in the boundary layer but that the air above is relatively clean.

Over land there is a pronounced diurnal variability and a great range of boundary layer depths: over the sea there is little diurnal change but much variability from day to day.

17.5.1 Unstable Boundary Layers

Given the original records it is possible to obtain a fair representation of unstable boundary layers from routine radiosonde ascents. Figure 17.9 shows a characteristic diagram obtained from the ascent at Ocean Weather Station (OWS) India (59°N, 19°W) at 2330Z on 10 March 1966. The variables plotted are the potential temperature θ and the specific humidity q, both of which are conserved in adiabatic motion and obey the simple law of mixtures. The q-θ diagram was used by Taylor (1917) as a tool for studying the atmospheric boundary layer and is sometimes called the Taylor diagram. The analogous S-θ diagram is widely used in oceanography, but the great convenience of the Taylor diagram has not been widely recognized in spite of a comprehensive review by Montgomery (1950).

For the ascent plotted it will be seen that the points corresponding to heights up to 908 mb are clustered together, indicating a high degree of mixing: higher up, the density gradient is definitely stable. The point representing air in contact with the sea is at a potential temperature 5°C higher than that typical of the mixed layer. The point corresponding to the observations at deck level theoretically would be expected to be on the line joining the mixed layer to the sea surface: that the surface values are lower is difficult to explain.

Figure 17.10 is a similar diagram from an ascent at Gan (0°41'S, 73°09'E). Some workers, influenced by Ekman's theory of the variation of wind with height, have predicted very deep boundary layers near the equator: that such a view is not borne out by observation goes some way toward demonstrating that the thickness of the boundary layer is determined more by the density structure.

Figure 17.11 gives the results of a special slowly rising ascent at OWS Julliet (52°30'N, 20°W). More
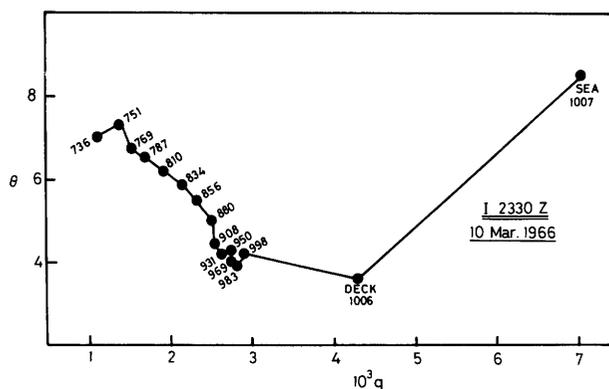
Figure 17.9 Characteristic diagram, OWS India (59°N, 19°W), on 10 March 1966.
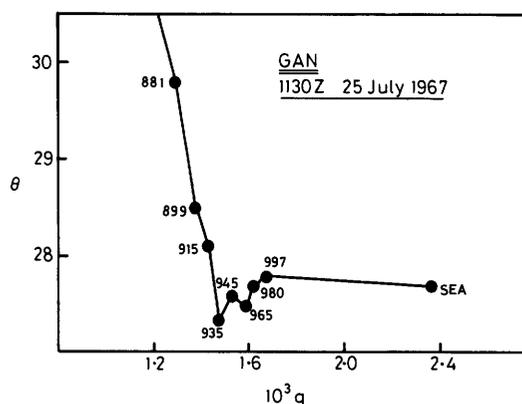
Figure 17.10 Characteristic diagram, Gan (0°41'S, 73°09'E), on 25 July 1967.

detail is given, but the structure is basically similar to that in figures 17.9 and 17.10. The wind profile at the same time shows that the wind varies slowly with height in the mixed layer, but that there is considerable shear at the boundary-layer top.

There remains a need for long-term studies of the character of the boundary layer over the sea so that their climatology can be established. A pilot study of the ascents at OWS India (59°N, 19°W) for March 1966 showed that more than half had reasonably well-defined unstable boundary layers. The boundary layer depth ranged from 200 to 2000 m, being at most weakly correlated with the vertical potential temperature difference between the sea surface and the mixed layer, which ranged from 0 to 9°C.

Even in convective conditions a well-mixed state with potential temperature independent of height is not always found, and it may be difficult to determine the depth of the boundary layer from the sounding. Also, when a well-mixed layer does exist it may be topped by a layer of relatively weak stability into which the stronger convective motions from below can penetrate a considerable distance.
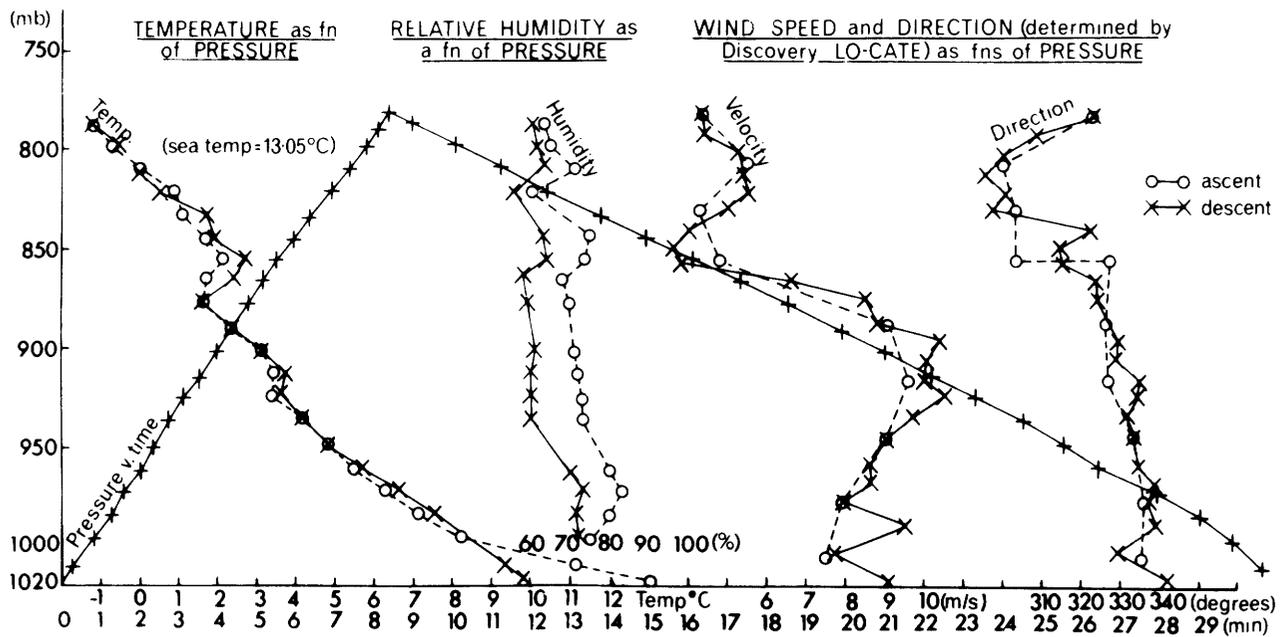
Figure 17.11 Records from LOCATE sonde (D.22) released from R.R.S. *Discovery* at 1915Z on 17 June 1970 near OWS Julliett, 52°30'N, 20°W. The record of pressure against time shows a rapid double-balloon ascent to a chosen height (780 mb), where one balloon is released and the other sinks at a slower speed (about 100 m min⁻¹) to the surface. Temperature, humidity, and wind are shown in relation to pressure for ascent and descent separately.

The thermals rising through a well-mixed layer commonly have values of specific humidity and potential temperature in their centers equal to those which would be produced by mixing equal parts of air from their environment and air from the surface. So, if the condensation level for such a mixture is within the well-mixed layer, cloud will form, its amount and development being related to the boundary-layer structure. If, on the other hand, the condensation level is above the well-mixed layer, condensation can occur only if the thermals are strong enough to penetrate the stable region above. This is the usual situation in the Trade Winds and tropics.

Once condensation has taken place the latent heat released adds to the clouds' buoyancy, so that in favorable cases the motion becomes unstable, and the clouds grow and may produce showers.

17.5.2 Buoyancy-Transfer Processes

As the surface is approached, the buoyancy forces have little dynamic effect, the temperature and humidity fluctuations being produced by vertical motions that they have not caused. From time to time air from the surface is lifted upward, probably in the form of a column or a sheet rather than a blob. As it rises it will be eroded at its edge by small-scale turbulence and become thinner. If the rising column survives long enough, its own buoyancy will begin to have an effect, so that in unstable conditions it will accelerate, being stretched and becoming even thinner as it rises. Some temperature traces made by Webb (see Priestley, 1967)

illustrate the thinning with height, and they are consistent with the idea of columns of warm air leaning downwind, since each active occurrence is first apparent at the greatest observation height. Figures 17.12 and 17.13, by Kaimal and Businger (1970), illustrate a case that has been studied further by Businger and Khalsa (1978).

After the rising warm air has acquired a vertical velocity appreciably greater than the turbulence at its level, it will cease to be eroded and will begin to entrain air into itself and grow (Elder, 1969). The motion may then have the character of a starting plume (Turner, 1969). Eventually the supply from below is cut off and the air transfers heat and water vapor, but is less efficient at transferring momentum: attempts have been made to predict the transfer coefficients theoretically (e.g., Richards, 1970), but the coefficients are not clearly established.

Since the velocity of individual thermals relative to their environment decreases with height, and since the environment must itself be sinking to compensate for the rising motion of the thermals, it is clear that the weaker thermals will be brought to rest at moderate heights, to be entrained into stronger ones. Thus it is possible for the cross section of each thermal to grow with height and yet the fraction of horizontal area occupied by rising air not to increase strongly with height.

The height at which a fair number of thermals can be said to be well formed and self-propelled is probably

H. Charnock
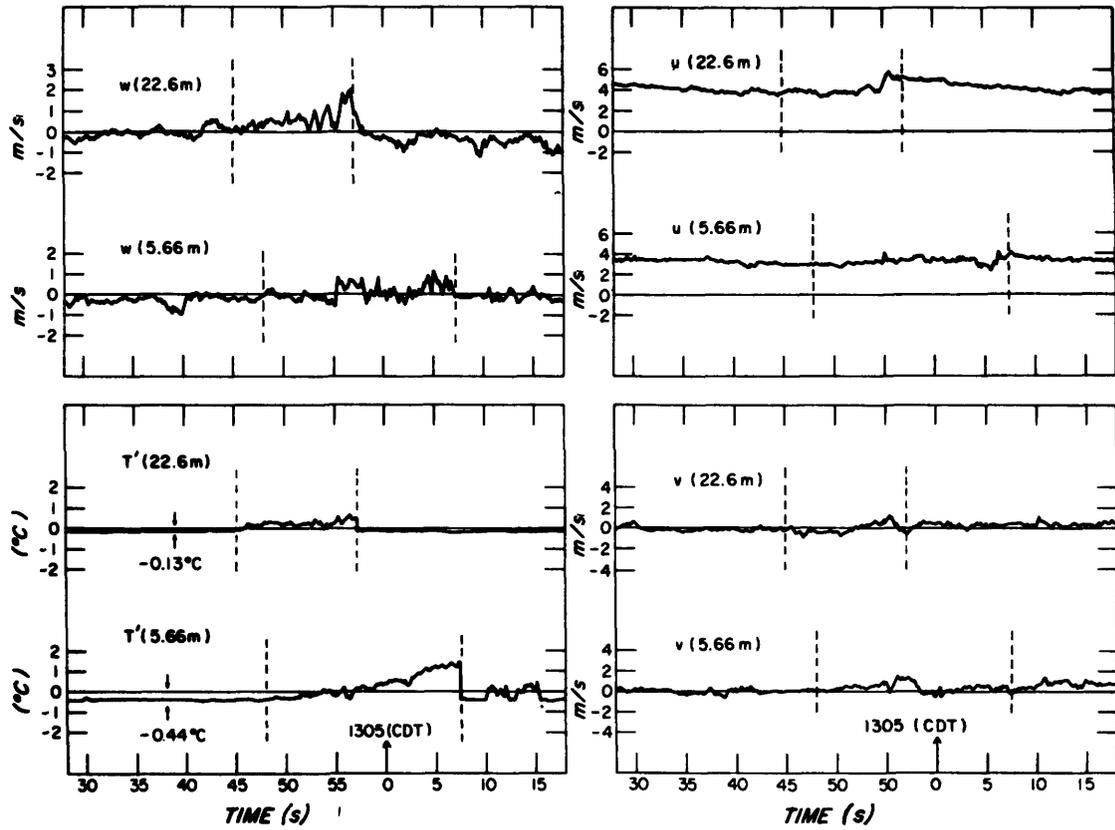
Figure 17.12 Traces of u, v, w and T (temperature) during passage of a convective plume. (Kaimal and Businger, 1970.)

$u_A = 5.0 \text{ m s}^{-1}$

$u_B = 3.5 \text{ m s}^{-1}$

$w_A = 2.0 \text{ m s}^{-1}$

$w_B = 1.0 \text{ m s}^{-1}$
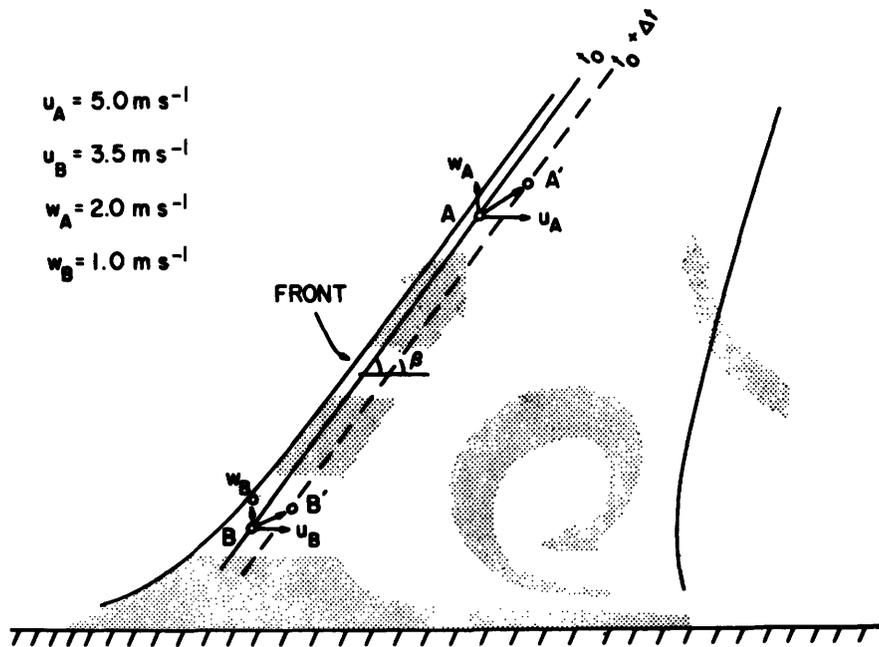
Figure 17.13 Two-dimensional model of a convective plume. (Kaimal and Businger, 1970.)

above the surface layer, where the temperature gradient and the wind shear are determined by the similarity rules. In particular the wind shear may be governed by the variation of the geostrophic wind with height. There is some evidence that when this is large there is a tendency for motions of scale comparable with the depth of the boundary layer to become organized into large longitudinal roll vortices. Given an appropriate condensation level, one would expect such motions to be visible in pictures of clouds taken from high-flying aircraft or from satellites, and many such images have been interpreted in this way; see, for instance, Agee and Dowell (1974) and Kuettner (1971). The patterns also depend on the general vertical motion due to convergence or divergence on the mesoscale or the synoptic scale.

The importance of clouds in the transport process is clear from studies that evaluate the heat or water budgets of the subcloud layer and the cloud layer separately. Riehl, Yeh, Malkus, and La Seur (1951) in a classical study found that as much as four-fifths of the water evaporated from the sea entered the cloud layer. This is a high value, to explain which it has been suggested that the transport is concentrated into localized areas where there are cloud groups or clusters. But the same sort of thing happens in polar outbreaks, with well-spaced clouds, so it seems likely that cumulonimbus clouds must suck up a large volume of the subcloud layer between them. Browning and Ludlam (1962) suggest a cumulonimbus model in which strong downdrafts partially compensate for the upflow, but in general there will be shrinking and subsidence in the subcloud layer in the space between clouds. The role of the heat and water-vapor fluxes from the surface is thus in the first instance to maintain the depth of the well-mixed layer rather than to feed directly into the layer clouds.

17.5.3 Stable Boundary Layers

Stable boundary layers, on the other hand, are difficult to investigate using routine observations. They are often relatively shallow, with small temperature differences, and since the transports of heat and water vapor are small, they have attracted little attention. There are few satisfactory sets of observations, but they can be interpreted as showing that heat is transferred to the surface until an almost linear gradient of potential density is formed from the surface to height h, where the difference in potential temperature $\Delta\theta$ is given roughly by

$$g\frac{\Delta\theta}{\theta}\,h/U_{10}^2 = 0.5. \qquad (17.22)$$

Hanna (1969) attributes (17.22) to Laikhtman (1961), and gives an example using O'Neill's data (Lettau and Davidson, 1957) that supports it.

Over the sea, figure 17.14, by Craig (1946), shows ascents made at three different fetches in warm continental air flowing out over colder sea. At the largest fetch

$$g\frac{\Delta\theta}{\theta}\,h/U^2 \approx 0.4.$$

One of the classical ascents made by Taylor (1914) on the S.S. *Scotia* provides another example (the others are not suitable because of fog), which is shown in figure 17.15. Here

$$g\frac{\Delta\theta}{\theta}h/U^2 \approx 0.35.$$

17.5.4 Wind in the Boundary Layer

Turbulent friction in the boundary layer causes the wind to deviate from its frictionless value, and earlier sections have shown how it increases rapidly, roughly as the logarithm of the height in the lowest few meters. From a height of 30 m or so there is usually relatively little change until the top of the boundary layer is reached. Sometimes there is a significant and rapid change with height at the top of the boundary layer until the frictionless value is attained.

The wind changes not only in speed but in direction also. Such changes were predicted by Ekman for the ocean and soon applied to the atmosphere by Akerblom and (some years later, independently) by Taylor. Because they took a constant value for the eddy viscosity K_M they got the well-known Ekman spiral for the hodograph. Perhaps more important is their deduction that in stationary conditions, when the boundary layer has a finite depth H, with zero stress above,

$$u_*^2 = \int_0^H f(V - V_g)\,dz,$$
$$0 = \int_0^H f(U - U_g)\,dz, \qquad (17.23)$$

where U_g, V_g are the components of the geostrophic wind.

This result is independent of the mechanism of transfer: it relates the surface stress to the cross-isobar transfer, and provides a basis for calculating the frictional convergence and so the mean vertical velocity at the top of the boundary layer. This, in turn, has an effect on the motion of the whole atmosphere. Unfortunately, conditions are rarely so simple as to allow a direct application of (17.23).

Much subsequent work has sought to use more complicated expressions for $K_M(z)$, to try to predict $K_M(z)$ theoretically, or to deduce it from observations. It is now known that the variation of the pressure gradient with height often has a large influence on the angle between the geostrophic and the surface wind; and that

H. Charnock
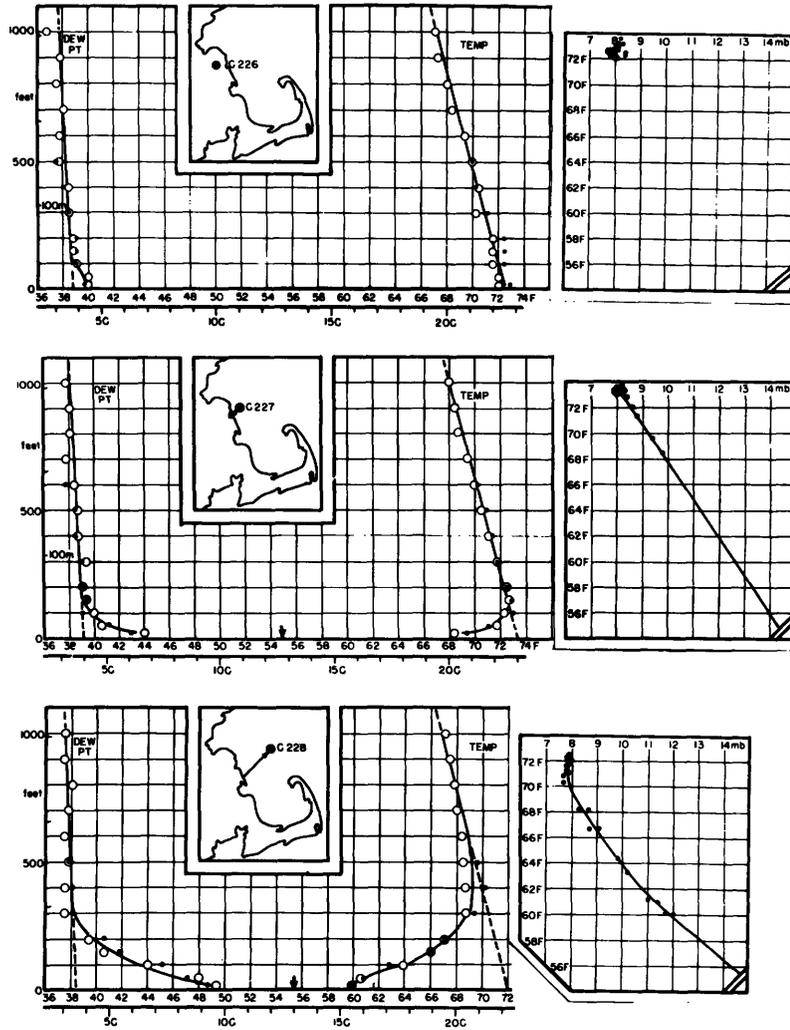
Figure 17.14 Modification of a warm continental air mass flowing over a colder sea, Massachusetts Bay, 18 October 1944, showing vertical distribution of temperature and dew-point and the corresponding Taylor diagrams. (Coordinates are potential temperature and potential vapor pressure.) Sea surface temperature indicated by arrows. (Craig, 1946.)
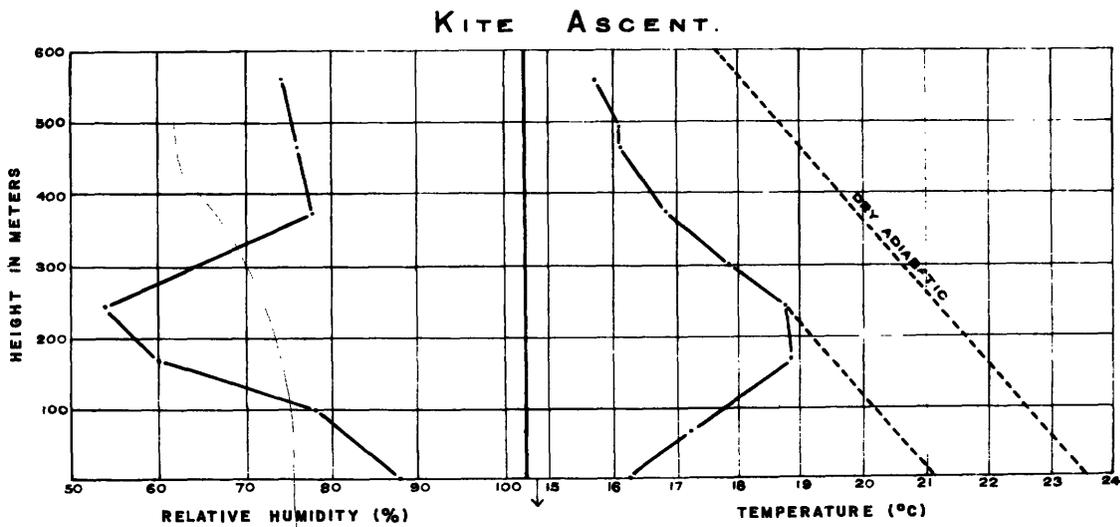
KITE ASCENT.

Figure 17.15 A kite ascent from S.S. *Scotia* at 44°39'N, 49°48'W, 29 July 1913. (Taylor, 1914.)

variations of K_M in time, or in the downstream direction, can lead to oscillations in which the flow in the middle of the boundary layer can increase considerably above its geostrophic value, giving rise to the so-called low-level jet.

Since it is known that near the surface $K_M = \kappa u_* z$ and that in neutral conditions this is a fair approximation up to 100 m or so, it is obviously worth examining the implications of assuming it true at all heights (Ellison, 1956). The results agree reasonably well with measured wind profiles, but this shows merely that they are insensitive to K_M above the surface layer. This does not vitiate, however, Ellison's demonstration that the thermal wind has a large effect.

Nevertheless in the (very rare) case when the stratification is so nearly neutral that it can be neglected, Kazanskii and Monin (1960, 1961) dealt with the problem in a convincing way. In these papers they introduced a similarity argument for the entire boundary layer that has since been discussed by Csanady (1967), Gill (1968), Blackadar and Tennekes (1968), Zilitinkevich (1969, 1970), and others. This is based on a combination of the surface-layer arguments, leading to the logarithmic wind profile together with a velocity defect law that asserts that

$$\frac{U}{u_*} = f(z/H) + \text{a velocity of translation.}$$

For the atmospheric boundary layer, the boundary layer thickness H is taken as u_*/f, where f is the Coriolis parameter. The result is, for neutral conditions

$$\frac{\kappa U_g}{u_*} = \ln\left(\frac{u_*}{fz_0}\right) + A,$$

$$\frac{\kappa V_g}{u_*} = B. \tag{17.24}$$

A reasonable value of A is 2 and of B is 5. Figure 17.16, by Lettau (1959), shows some of the earlier results.

In nonneutral conditions the relation for a transferable scalar is

$$\frac{\kappa(\Theta - \Theta_0)}{\theta_*} = \ln\left(\frac{u_*}{fz_\theta}\right) + C, \tag{17.25}$$

but in the nonneutral case A, B, and C are no longer constants but functions of $\mu \equiv u_*/fL$.

Valiant attempts to measure $A(\mu)$, $B(\mu)$, and $C(\mu)$ have been made by Clarke (1970) and others over land. The results are very scattered, possibly because of effects of time and space variability.
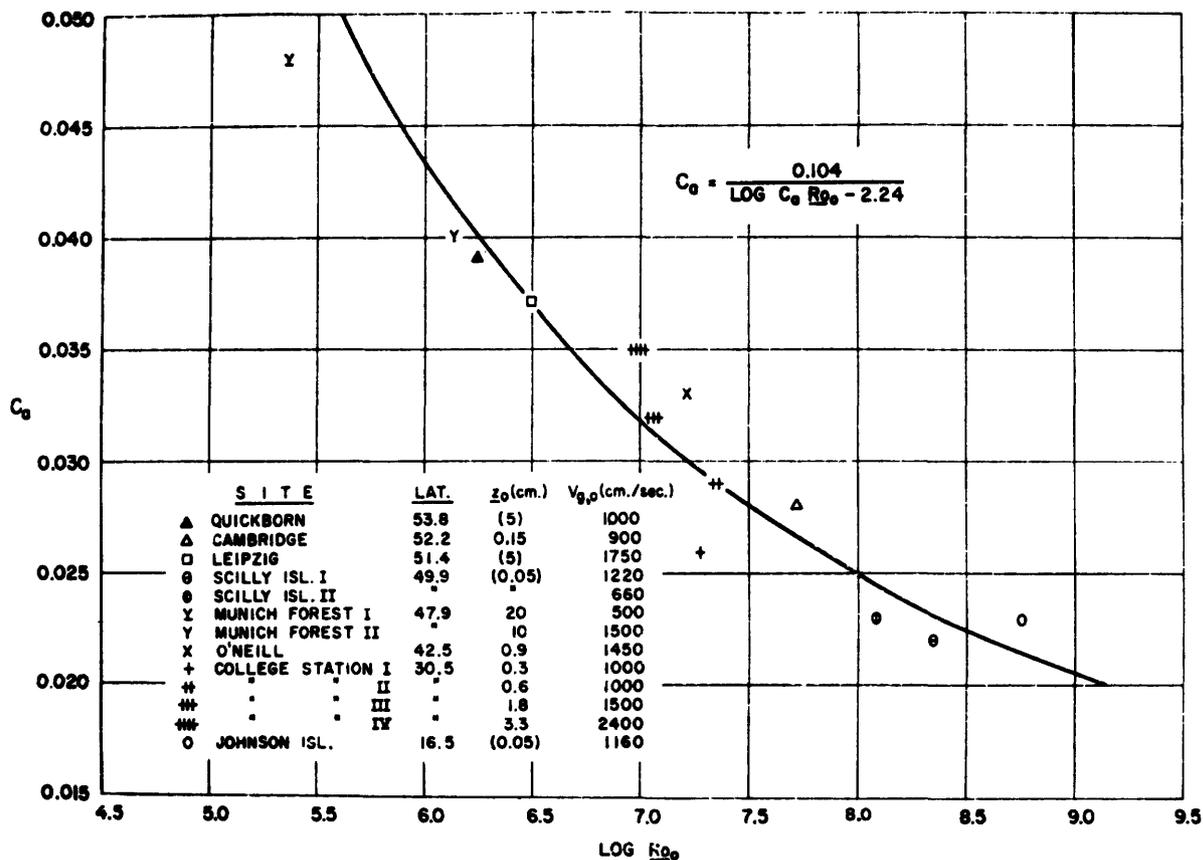
Figure 17.16 Geostrophic drag coefficient versus surface Rossby number. $C_a = u_*/|V_g|$, $Ro_0 = |V_g|/(fz_0)$. (Lettau, 1959.)

H. Charnock

There seems to be no way to avoid the need for an evolving model of the boundary layer in which the height of the top will be predicted. This will depend on advection, on the (frictional and frictionless) convergence, and on the entrainment of the air above. In this sense the early single-point measurements (Sheppard, Charnock, and Francis, 1952; Charnock, Francis, and Sheppard, 1956) and others well described by Roll (1965) are of limited value. More recent studies have been large acronymic projects like ATEX (Augstein, Schmidt, and Ostapoff, 1974), BOMEX (Holland and Rasmusson, 1973), GATE, AMTEX (Ninomiya, 1974) and JASIN (Taylor, 1979), from which no simple result has yet been distilled.

A climatological study has been made by Findlater, Harrower, Howkins, and Wright (1966): this and related work is reported by Sheppard (1970), from whom figure 17.17 is taken. The geostrophic drag coefficient implied by (17.24) must also be consistent with the requirements of the angular-momentum balance of the earth, and La Valle and Di Girolamo (1975) have thus found a mean value $(= u_*^2/|V_g|^2)$ of 0.41×10^{-3}.

Even in cloud-free conditions the dynamics of the atmospheric boundary layer is complicated: it is not yet clear which are the most important transfer processes or how they can be dealt with.

17.5.5 The Upper Boundary Layer of the Ocean

The near-surface boundary layer of the ocean has much in common with that of the atmosphere. It is most obvious from the vertical density structure: more or less well-mixed layers are to be found near the surface over most of the ocean most of the time. As in the atmosphere the velocity structure is not well known (it is difficult to measure currents in the presence of waves), but the simple Ekman-type distributions are rarely found.

Like the atmospheric boundary layer, the oceanic boundary layer is maintained by a combination of advection, surface fluxes, and entrainment at the lower surface. Because vertical gradients are much bigger than those in the horizontal, the advection can often be neglected: the basis of the resulting one-dimensional models is well described by Niiler and Kraus (1977), and details of the complicated mixing processes are given by Turner (chapter 8).
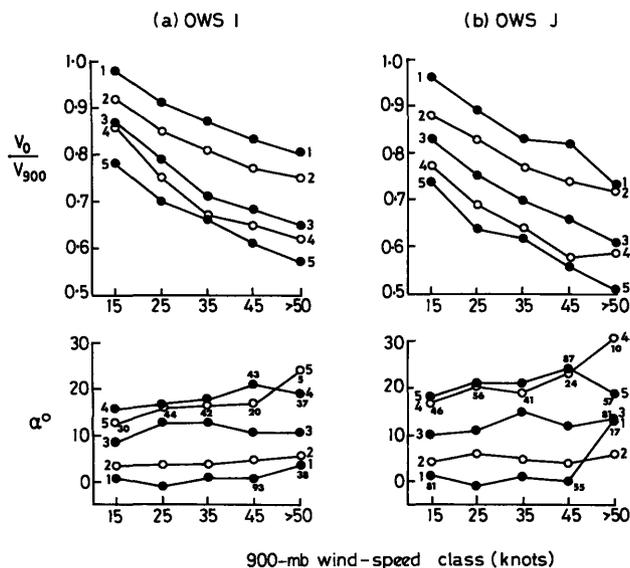
Figure 17.17 The variation of the ratio between the wind speed at the surface (V_0) and at 900 mb (V_{900}) and of the angle between them (α) in relation to V_{900} mb and the mean lapse rate from surface to 900 mb at OWS India and Julliett. The points refer to classes in wind speed (kt): 10-19, 20-29, 30-39, 40-49, >50, and in lapse rate (°F/1000 ft = 1.69°C/km): >5.5 (1), 5.4 to 4.0 (2), 3.9 to 2.5 (3), 2.4 to 1.0 (4), 0.9 to −0.5 (5). Smaller lapse rates and lower wind speeds excluded. Lapse class shown against end of curves. Number of observations in each class when less than 100 shown in parentheses. (Due to Findlater et al., 1966.)